Viewpoint Selection for Molecular Visualization: Analysis and Applications

Vincent Larroque[1], Maxime Maria[1], Stéphane Mérillou[1] and Matthieu Montes[2,3]
[1]*Laboratoire XLIM, UMR CNRS 7252, Université de Limoges, France*
[2]*GBCM - Laboratoire Génomique, Bioinformatique et Chimie Moléculaire, EA7528, Conservatoire National des Arts et Métiers, Hésam Université, France*
[3]*Institut Universitaire de France (IUF), France*

Keywords: Molecular Visualization, Viewpoint Selection, Virtual Tours.

Abstract: Molecular systems are often visually complex and abstract. It can be difficult, even for experts, to explore and find meaningful viewpoints. Research in viewpoint selection methods has mainly focused on general real-world objects and only a few works tackled molecular scenes. In this paper, we present a study of 20 state-of-the-art viewpoint selection methods from the general field, applied to molecular visualization. Our goal is to determine if these methods can find two important geometrical configurations for molecules. Additionally, we propose an automatic generation of informative and visually pleasing molecular tours to help the study and the communication around molecules.

1 INTRODUCTION

The study of molecular systems, for instance for drug design, has been increasingly relying on computer visualization as it simplifies the exploration, analysis, and understanding of their properties and actions. Visualization software also enables experts to share the results of their studies more easily between them or with the general public (Olson, 2018).

Molecules can be represented in various ways, each providing specific information about their properties (Kozlíková et al., 2017). Figure 1 shows the geometric diversity of representations that can be used. *Ball & Stick* (figure 1a) displays the atoms and their covalent bond as spheres and cylinders; *van der Waals* (figure 1b) only shows atoms as spheres with a radius proportional to their van der Waals radius; *Solvent Excluded Surface* (figure 1c) gives the boundary of the molecular volume regarding a solvent; *Cartoon* (figure 1d) describes the secondary structure of the molecule with ribbons, arrows, and coils.

Molecular systems are visually complex and abstract objects, whatever their representation. It is thus difficult, even for experts, to explore them to find meaningful points of view. An automatic viewpoint search tool would therefore make their work easier and increase their productivity. Despite this potentially useful application, only a few works have tackled this issue.

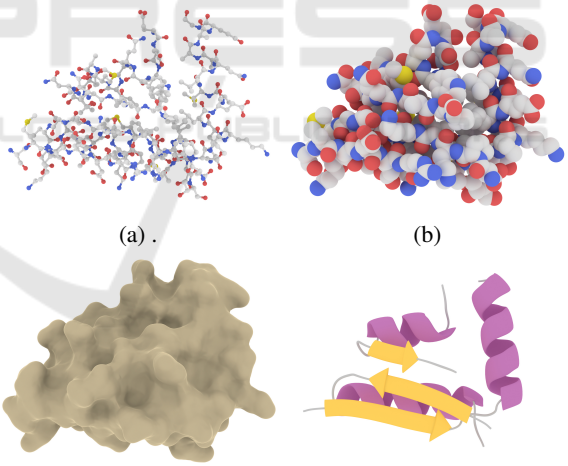

Figure 1: Different molecular representations of the same molecule: (a) *Ball & Stick*; (b) *van der Waals*; (c) *Solvent Excluded Surface*; (d) *Cartoon*.

Viewpoint selection methods have been vastly studied to find good views of general "real-world" objects, for instance for movies, video games, or computer-aided design (Bonaventura et al., 2018). However, most of these works have not been tested for molecular visualization which makes it difficult to develop new dedicated methods.

Larroque, V., Maria, M., Mérillou, S. and Montes, M.
Viewpoint Selection for Molecular Visualization: Analysis and Applications.
DOI: 10.5220/0012383300003660

In *Proceedings of the 19th International Joint Conference on Computer Vision, Imaging and Computer Graphics Theory and Applications (VISIGRAPP 2024) - Volume 1: GRAPP, HUCAPP and IVAPP*, pages 58-69
ISBN: 978-989-758-679-8; ISSN: 2184-4321

In this paper, we propose a global study of previous general methods to evaluate their capacity to find points of interest in molecular scenes. In addition, we use the results of this analysis to propose a tool for automatically creating tours of important features of molecular systems.

In summary, our main contributions are:

- An analysis of general state-of-the-art viewpoint selection methods for general objects applied to molecular visualization.
- A benchmark of the ability of these methods to detect specific geometrical configurations for molecules.
- A method to generate informative tours of molecular systems going through these geometrical configurations.

This paper is organized as follows: section 2 presents the state-of-the-art in viewpoint selection and automatic tour creation. Section 3 proposes an analysis of previous works in the context of molecular visualization. Section 4 describes the automatic tour creation process. Finally, section 5 concludes and gives some future work directions.

2 RELATED WORK

The search for informative viewpoints is closely related to perception. Many studies have concluded that a meaningful viewpoint tries to display most of an object to enable quick recognition (Blanz et al., 1999). For data visualization, domain-specific features are important to find and display as they can help to understand a given scene. Animation tours are also a powerful tool to improve comprehension, especially for complex data as in medicine. (Preim and Meuschke, 2022).

2.1 Viewpoint Selection

One of the first works to deal with viewpoint selection was by (Kamada and Kawai, 1988). They tried to minimize the number of visible faces with parallel edges using an orthographic projection to help object understanding. However, they did not aim to find a "good" viewpoint, *i.e.*, bringing interest to the viewer. (Plemenos and Benayada, 1996) presented metrics based on the projected area of an object to try to capture viewpoints showing most of the objects. Finding good points of view is related to the amount of information they provide about the scene. As such, (Vázquez et al., 2001) introduced a new metric based on (Shannon, 1948)'s information theory: *Viewpoint entropy*. Information theory has subsequently been widely used to design new metrics. The surveys of (Secord et al., 2011) and (Bonaventura et al., 2018) present and evaluate most of them.

Recently, deep learning has been used to find good viewpoints for general objects. (Schelling et al., 2021) proposed a viewpoint selection method based on learning previous metrics which is insensitive to model resolution, faster to compute, and as reliable as other state-of-the-art works. (Hartwig et al., 2022) conducted a user study on 3220 models, enabling them to present the first view quality metric solely based on human preferences. They also showed that their method performs better than previous works but requires a huge dataset of manually selected good viewpoints.

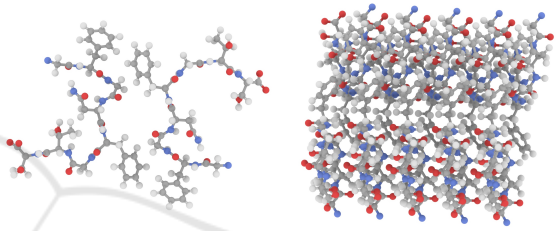

(a) (b)

Figure 2: (a) The alignment, where only the foreground is visible. (b) Another viewpoint of the same molecule.

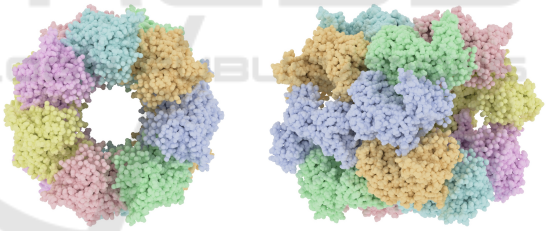

(a) (b)

Figure 3: (a) The tunnel, with a hole going through the molecule. (b) Another viewpoint of the same molecule.

Viewpoint selection for molecular systems has not received much attention despite its potentially useful applications. (Vázquez et al., 2002) adapted *Viewpoint entropy* for molecular scenes. They try to find viewpoints where there is an alignment between elements of a molecule (figure 2a), or where most elements can be seen (figure 2b). This process is done using an orthographic camera, as usual in scientific visualization, and a molecule with the *Ball & Stick* representation. (Doulamis et al., 2010) extended Vázquez's work by adding semantic information to the molecules in order to select more relevant and informative views. They created an online platform for experts to visualize and select the best

views given by a non-linear classifier which was continuously trained from their input. (Heinrich et al., 2016) adapted *Viewpoint entropy* to use some information specific to the *Cartoon* representation. They conducted a quantitative study with experts and non-experts to determine what a good viewpoint is for molecules. They concluded that both a viewpoint showing most of the molecule (figure 3b) and a viewpoint exposing a tunnel (figure 3a), where a hole going through the molecule can be seen, are important for improved understanding.

In this paper, we extend the preliminary study of (Larroque et al., 2023) by adapting and analyzing most metrics from previous works applied to molecular visualization. Our goal is to find which metrics are interesting for tunnel and alignment detection and also evaluate their ability to be used for molecular tour creation.

2.2 Automatic Tour Creation

Creating a good camera tour around objects is tied to the viewpoint selection process. (Barral et al., 2000) created an iterative algorithm using metrics from (Plemenos and Benayada, 1996) to generate a path from consecutive steps that are selected according to their view quality. However, their method resulted in a jerky movement. (Sokolov et al., 2006) improved this process by adding inertia factors to the camera movement to smooth out sharp turns. Later (Saleem et al., 2007) presented a method that only uses some key viewpoints to create a smooth tour of general objects using cubic splines. (Secord et al., 2011) maximizes the quality of a periodic orbit using the gradient of metrics scores.

Viewpoint selection has also been used in other works to create complete scene tours. (Sokolov and Plemenos, 2008) compute some key viewpoints of a scene that are linked together using scene topological and semantic knowledge. (Xie et al., 2018) generate paths for quadrotor videography by chaining local moves that are computed using saliency fields on different landmarks and global moves between them. Both works solve a Traveling Salesman Problem (TSP) to find the shortest path connecting key viewpoints that were computed using viewpoint quality metrics.

For molecular visualization, (Kouřil et al., 2021) presented an automatic documentary creation process for huge scenes containing thousands of individual molecules. Their method is based on a script that can either be written by a user or generated using online available information. They then create a tour from the script that goes through key parts of the visualized system. Occlusion issues are solved by using culling planes, trading off contextual information for easier navigation and visualization. The tour creation process was improved by (Alharbi et al., 2021) as they proposed a method to navigate through empty space when possible and hide unavoidable occluding elements instead of using culling planes like Kouřil. While these works provide good results for their use case, they do not take viewpoint quality into account and are not designed to handle unknown molecules.

We propose to improve (Larroque et al., 2023) work on molecular tour creation by solving a TSP over key viewpoints and focusing on the most important areas, similar to (Saleem et al., 2007). Additionally, we take some animation principles into account to create both an informative and visually pleasing tour.

3 METRICS ANALYSIS AND EVALUATION

Viewpoints are selected using metrics that give a score according to the information visible on a given image. In this section, we analyze 20 state-of-the-art metrics from previous works to evaluate their ability to identify two specific geometrical configurations of molecules: alignments (figure 2) and tunnels (figure 3). These metrics are divided into five categories defined in (Bonaventura et al., 2018) and (Secord et al., 2011): Silhouette (section 3.2), Surface (section 3.3), Depth (section 3.4), Stability (section 3.5), and High-level (section 3.6). More details on each studied metric are given in the appendixes A to E.

3.1 Analysis Introduction

Process. Candidate viewpoints are sampled around the molecule using a bounding icosahedron of 642 vertices as a trade-off between computation time and covered space around the molecule (an example icosahedron can be seen on figure 4a). Images used to compute the metrics are rendered from each vertex with an orthographic camera facing the center. The viewport size is set to be able to fit the whole bounding sphere of the molecule on the screen.

Image resolution has a strong impact on the amount of visible information, and therefore on the metrics score. Indeed, a lower image resolution leads to more elements covering a single pixel. It is thus important to determine the appropriate pixel count and aspect ratio when trying to find the best viewpoint. We evaluate three factors over several resolutions using a common 16:9 aspect ratio. We choose

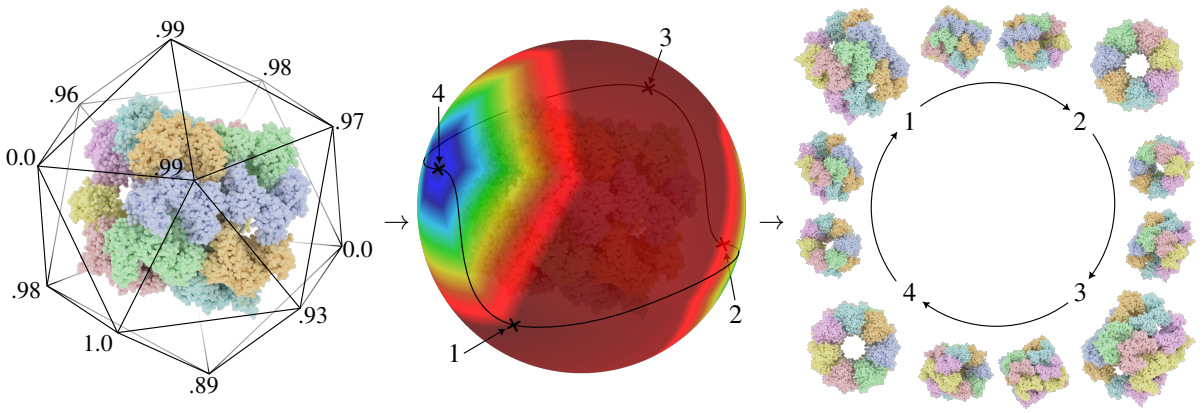

(a) (b) (c)

Figure 4: Tour creation for a molecule: (a) the icosahedron used to sample viewpoints with computed scores; (b) the spherical heatmap generated with scores from (a); (c) key (numbered) and intermediary viewpoints of the resulting video.

the 3840×2160 (2160p) resolution as a baseline for comparisons, as it's common for high-quality images.

The results can be seen in figure 5:

- *Time gain vs 2160p* is the relative rendering time, compared to 2160p. The gain decreases almost linearly with the resolution. This factor does not take metrics computation into account.
- *Avg. visible elements vs 2160p* is the average number of elements visible from all viewpoints, compared to 2160p. A higher number of visible elements per image means that metrics have more information and provide more accurate results.
- *Total visible elements %* corresponds to the number of unique elements of the molecule seen at least once. It tends to be stable after 720p.

Taking these elements into account, we choose to render the scene with a 1280×720 (720p) image resolution, as the best trade-off between available information and computing cost.

Evaluation. Each of the 20 studied metrics has been tested from each viewpoint on the icosahedron (figure 4a), using a dataset of 33 molecules for tunnels and 30 for alignments. The molecules PDB IDs (Berman et al., 2000) are given in the appendix F. The generated images were manually examined to determine if the geometrical configuration evaluated was visible or not. We use the *Ball & Stick* representation to identify alignments as it helps to see repeating patterns (Vázquez et al., 2002) and is thus suitable for this feature. A viewpoint is considered valid if there is an alignment between elements of the molecule (figure 2a). For the tunnel, we use the *van der Waals* representation for its simplicity and ability to highlight

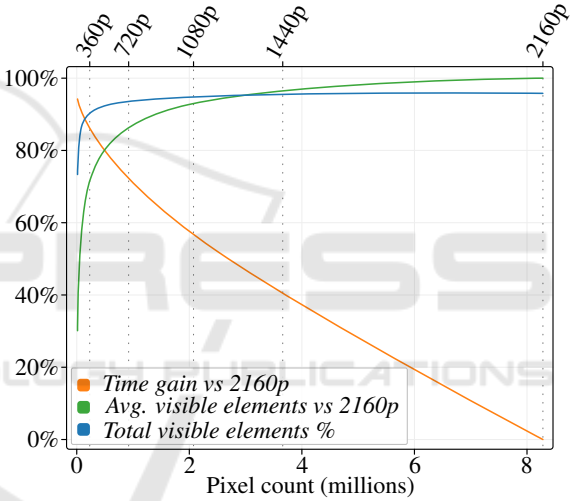

Figure 5: Analysis of different pixel counts for images rendered with orthographic camera using a 16:9 aspect ratio.

it. A viewpoint with a tunnel is considered valid if it is on the view axis such as on figure 3a.

To analyze the resulting data, we evaluate each metric by measuring the following attributes:

- Accuracy: it gives the overall ability of a metric to detect a given geometrical configuration either on its highest or lowest scoring viewpoint.
- Consistency: the ability of a metric to reliably find a given geometrical configuration exclusively on its highest or lowest scoring viewpoint.

3.2 Silhouette Metrics

This category uses the silhouette of an object to compute the score of a viewpoint and can be used on molecules without changes, capturing its overall

shape. Figure 6 gives the accuracy and consistency for metrics in this category and their definition are given in appendix A.

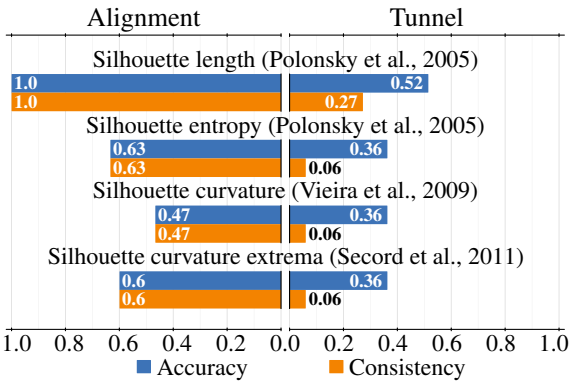

Figure 6: Results of accuracy and consistency for silhouette metrics for both evaluated geometrical configurations.

Alignment. The only silhouette metric capable of consistently finding the alignment is *Silhouette length*. Strong alignment means fewer elements are visible, and therefore the number of pixels making up the silhouette is lower. The other metrics, which rely on the turning angles between consecutive pixels, are not accurate or consistent. This is because, as atoms are spheres, a lot of curves are added to the silhouette making them unable to capture the external shape.

Tunnel. *Silhouette length* performs better than the others because the tunnel opening adds a big hole to the silhouette. Thus, the number of pixels increases, and the highest-scoring viewpoints correspond to visible tunnels. However, depending on the molecule shape, nothing guarantees that the longest silhouette is on the tunnel side. The other metrics perform worst for the same reason as the alignment: the silhouette does not capture the external shape of the molecule.

3.3 Surface Metrics

Metrics in this category initially used the surface of the triangles in screen space to compute a score for an object. For molecules, the projected surface of the elements (atoms and bonds) is used. The accuracy and consistency for metrics in this category are found in figure 7 and they are defined in appendix B.

Alignment. Surface metrics can constantly find the alignment. Indeed, using an orthographic camera, the viewpoint with the alignment results in the smallest projected surface (figure 2a). The exception is *Information* I_3 which does not perform well because it tries

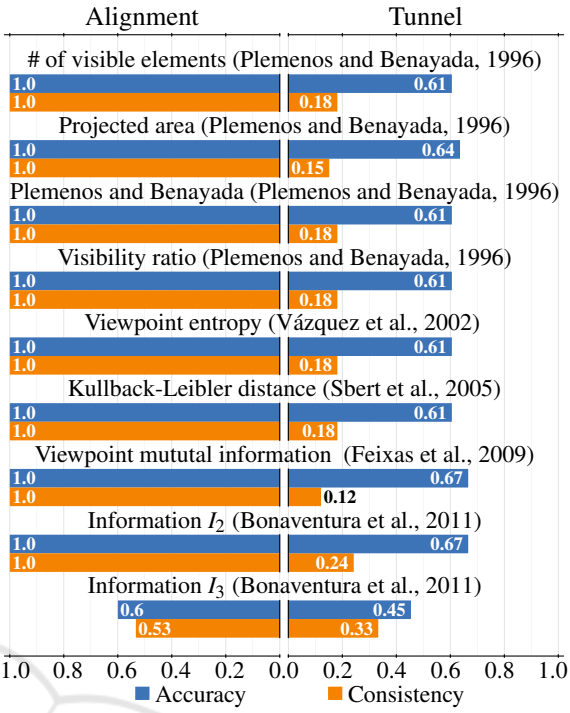

Figure 7: Results of accuracy and consistency for surface metrics for both evaluated geometrical configurations.

to capture viewpoints where elements are the most informative (*i.e.*, visible on many viewpoints). However, with *Ball & Stick* a lot of elements could be visible from many points of view.

Tunnel. Most metrics have slightly above average accuracy but bad consistency. Indeed, they are designed to identify viewpoints showing a lot of elements or with a high projected surface. This makes them unable to generalize around tunnels, which can be anywhere in a molecule and not only on the restricted cases of surface metrics.

3.4 Depth Metrics

Depth metrics use the depth map of the image to characterize the surface layout of the molecule. The results for metrics in this category can be found in figure 8 and their definitions are given in appendix C.

Alignment. *Maximum depth* performs perfectly for alignment because the farthest elements are hidden when a molecule is aligned. *Stoev and Straßer* has the same results because it uses maximum depth and the projected surface. The two other metrics of this category use entropy to analyze the overall depth range. They give the worst results because alignment does not have a significant impact on entropy.

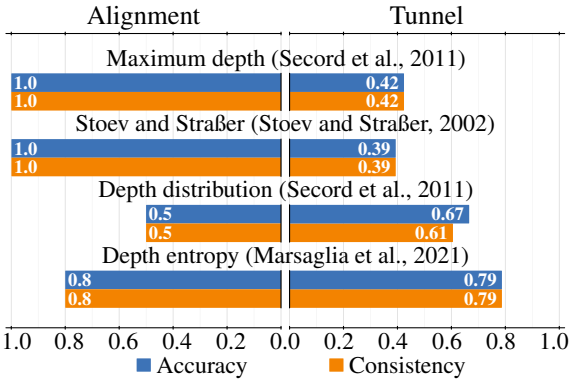

Figure 8: Results of accuracy and consistency for depth metrics for both evaluated geometrical configurations.

Tunnel. As *Maximum depth* and *Stoev and Straßer* seek the maximum depth in an image, they only allow finding a tunnel when it is perfectly on the view axis. *Depth distribution* and *Depth entropy* work better as they analyze the depth: when a tunnel is found the range of values is balanced, making both metrics have their lowest score.

3.5 Stability Metrics

Stability metrics compare a viewpoint to the others to return a score based on their differences. The accuracy and consistency are found in figure 9 and the two definitions are given in appendix D.

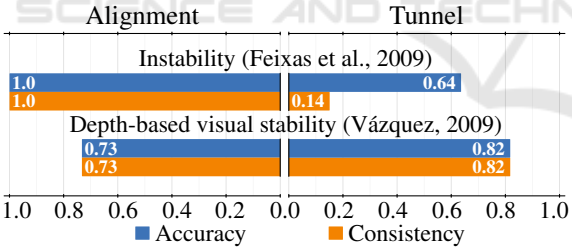

Figure 9: Results of accuracy and consistency for stability metrics for both evaluated geometrical configurations.

Alignment. An aligned viewpoint is unstable by nature: a small change in camera orientation leads to a big change on the screen. *Instability* thus provides perfect results in this case. *Depth-based visual stability* is not as efficient because, similarly to *Depth entropy* (section 3.4), it computes scores based on an analysis of the overall depth range, so alignment does not have much effect.

Tunnel. *Instability* is not consistent in this case. For instance, when molecules have short tunnels (as in a torus shape), most of the same elements are visible from everywhere. Longer tunnels are, however, unstable because the neighbors will reveal hidden elements in the tunnel interior by moving off axis. *Depth-based visual stability* shares the strengths of depth metrics (*i.e.*, an analysis of the full range of depth values) and compares a viewpoint to the others so it is more accurate and consistent than other comparable metrics.

3.6 High-Level Metrics

Based on the works of (Trellet et al., 2015) we introduce a new metric: *Largest cone of view*. Like the authors, we convert the atom's positions from Cartesian coordinates to spherical ones, ignoring the radial distance. Finally, we compute the Voronoï diagram of these points, giving us the set of circumcircles. Originally, the authors positioned the camera in the center of the biggest circumcircle to display the tunnel. However, viewpoint selection metrics in this study are defined as functions that return a score for any viewpoint. This is why we propose the formula in appendix E, which shows tunnels on its highest score. The accuracy and consistency for this metric are found in figure 10.

As this metric is conceived around tunnel detection, it has the worst performance for alignment, being unable to find any. For the tunnel, it reliably finds this configuration about 80% of the time.

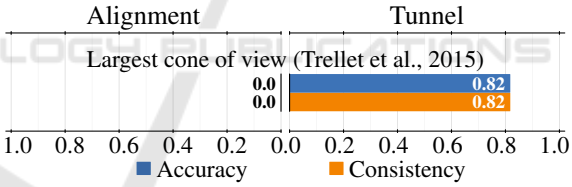

Figure 10: Results of accuracy and consistency for high-level metrics for both evaluated geometrical configurations.

3.7 Conclusion

For alignment, most metrics have perfect accuracy and consistency and can be used to search for this feature. Among them, silhouette, surface and depth metrics are cheap to compute because they only need to apply a formula for each pixel. In contrast, *Instability* is more costly because it requires comparing viewpoints between them.

In the case of tunnels, three metrics have both accuracy and consistency of about 80%. *Largest cone of view* is quite expensive as it needs to compute Voronoï diagrams. *Depth-based visual stability* is even more costly as it requires compressing hundreds of depth images to compute a score. Thus, *Depth entropy* is considered the best metric to find tunnels.

This study also reveals that there are no metrics able to reliably provide perfect results for both alignment and tunnel detection. Such metric would be interesting when analyzing unknown molecules. *Depth entropy* is currently the closest to achieving this goal with around 80% consistency for both configurations.

Computing metrics for each candidate viewpoint can be used to create a heatmap of interesting zones around molecules (figure 4b). It could be used as a non-intrusive way to guide the gaze of users when they analyze molecules, helping their studies.

4 MOLECULAR TOUR

In this section, we present how we can use the results of the best viewpoint selection process to create molecular tours.

4.1 Path Creation

To create the tour, we compute a path going through the most meaningful viewpoints around a molecule. We start with a set $\mathcal{C}$, composed of viewpoint candidates sampled around the molecule using the icosahedron (figure 4a). The tour path is created following these steps:

1. We normalize the score values in $\mathcal{C}$.
2. We arbitrarily select the 20% lowest and highest scoring candidates (according to the used metric).
3. We iteratively select key viewpoints by spreading candidates by a ϕ angle in ascending or descending scores, depending on the case.

Algorithm 1 gives more details for the selection of the highest score viewpoints. This algorithm is also used for lowest score viewpoints by considering candidates with a score inferior to 0.2 and sorting them in ascending order.

Finally, to find the shortest loop around the molecule, we solve a TSP on the combined key candidate viewpoints to find the best connection between them. An example of connected key viewpoints for a molecule can be seen in figure 4b.

Data: Candidates set $\mathcal{C}$
Result: Key candidates set $\mathcal{K}$
$\mathcal{C} \leftarrow \{\forall c \in \mathcal{C} \mid score(c) > 0.8\}$;
Sort candidates set $\mathcal{C}$ by descending scores;
// Add highest score candidate as key.
$\mathcal{K} \leftarrow \{\mathcal{C}[0]\}$;
$\mathcal{C} \leftarrow \mathcal{C} \setminus \{\mathcal{C}[0]\}$;
foreach $c \in \mathcal{C}$ **do**
  valid $\leftarrow$ true;
  /* Checks if c is properly spaced against key viewpoints. */
  foreach $k \in \mathcal{K}$ **do**
    /* Angle between c and k relative to the icosahedron center. */
    if $angleBetween(c,k) < \phi$ **then**
      // Remove from candidates.
      $\mathcal{C} \leftarrow \mathcal{C} \setminus \{c\}$;
      valid $\leftarrow$ false;
      break;
    end
  end
  if *valid* **then**
    // Add as key.
    $\mathcal{K} \leftarrow \mathcal{K} \cup \{c\}$;
    $\mathcal{C} \leftarrow \mathcal{C} \setminus \{c\}$;
  end
end

Algorithm 1: Key candidate viewpoint selection for highest scores (> 0.8).

4.2 Animation

To create an informative and pleasing animation of the computed path, we use some principles described in the analysis of (Lasseter, 1987):

1. Slow in and out: the camera speed is animated such as it accelerates and decelerates when going from one point to another.
2. Staging: using a non-linear slow in and out, we can fly more quickly over uninteresting areas while slowing down to a stop at key viewpoints. This makes the viewer implicitly informed about what parts of the tour are more important.
3. Arcs: by running the animation on the bounding sphere, the trajectory is naturally an arc. Also, we get a smooth trajectory by using a Catmull-Rom (Catmull and Rom, 1974) spline to connect the key viewpoints.

Finally, according to (Sokolov and Plemenos, 2008), the animation should not be very long. Our tour duration can be fully configured according to preferences or applications by adjusting the camera speed.

4.3 Results

For this paper, we set $\phi = 100$ in algorithm 1 to get at most three viewpoints for high and three for low scores, resulting in at most six key viewpoints. Finally, we set the camera speed to get an animation of about 50 seconds.

Our analysis (section 3) shows that several metrics have perfect results for finding alignments. However,

to create tours, it is also important to have viewpoints that display most elements of a molecule. For this reason, metrics like *Maximum depth* are not adapted.

For the tunnel, two of the three best metrics are computationally expensive without giving much better results. We thus choose *Depth entropy* to create molecular tours of this feature.

Figure 4c shows several frames extracted from a molecular tour. The tour goes through key viewpoints that either show the tunnel or most elements of the molecule. Additionally, we provide videos of tours for the two geometrical configurations studied (*i.e.*, tunnel and alignment) in supplemental materials.

5 CONCLUSION AND FUTURE WORKS

This article proposes an analysis of general state-of-the-art viewpoint selection methods applied to molecular visualization. Metrics from these works are analyzed on their ability to consistently find the tunnel or alignment geometrical configurations of molecules. This study reveals that for the alignment, most surface metrics can be used as they are perfectly accurate and consistent. For the tunnel, *Depth entropy* is the best trade-off between computation time and the ability to consistently show the tunnel. Finally, our study reveals that there is no existing metric capable of identifying both configurations reliably.

We also propose a simple method to create tours of interesting points around the molecules. With careful selection of candidate viewpoints, and by using splines to obtain a smooth path we can create an informative and visually pleasing tour respecting some important animation principles. These molecular tours can help users identify key areas and improve their understanding of such complex objects.

An interesting future work could focus on creating specific metrics to detect other important features of molecules, geometrical or not. Combining metrics and studying their behavior for molecular visualization could also be valuable. According to the application, a user study may be necessary to assess the relevance of the designed metric. Finally, our tour only shows the exterior of the molecule. Creating a view quality-based tour for the whole molecular system would help to understand the visualized scene better.

ACKNOWLEDGMENTS

Vincent Larroque is supported by institutional grants from the National Research Agency under the Investments for the future program with the reference ANR-18-EURE-0017 TACTIC and a fellowship from Qubit Pharmaceuticals. Matthieu Montes is supported by the European Research Council Executive Agency under grant numbers 640283 and 101069190.

REFERENCES

Alharbi, R., Strnad, O., Luidolt, L. R., Waldner, M., Kouřil, D., Bohak, C., Klein, T., Gröller, E., and Viola, I. (2021). Nanotilus: Generator of Immersive Guided-Tours in Crowded 3D Environments. *IEEE Transactions on Visualization and Computer Graphics*, 29(3):1860–1875.

Barral, P., Dorme, G., and Plemenos, D. (2000). Scene understanding techniques using a virtual camera. In *Eurographics 2000 - Short Presentations*. Eurographics Association.

Berman, H. M., Westbrook, J., Feng, Z., Gilliland, G., Bhat, T. N., Weissig, H., Shindyalov, I. N., and Bourne, P. E. (2000). The Protein Data Bank. *Nucleic Acids Research*, 28(1):235–242.

Blanz, V., Tarr, M. J., and Bülthoff, H. H. (1999). What Object Attributes Determine Canonical Views? *Perception*, 28(5):575–599.

Bonaventura, X., Feixas, M., and Sbert, M. (2011). Viewpoint Information. *21st International Conference on Computer Graphics and Vision, GraphiCon'2011 - Conference Proceedings*.

Bonaventura, X., Feixas, M., Sbert, M., Chuang, L., and Wallraven, C. (2018). A Survey of Viewpoint Selection Methods for Polygonal Models. *Entropy*, 20(5):370.

Catmull, E. and Rom, R. (1974). A Class of Local Interpolating Splines. In Barnhill, R. E. and Riesenfeld, R. F., editors, *Computer Aided Geometric Design*, pages 317–326. Academic Press.

Doulamis, N., Chronis, E., Doulamis, A., Miaoulis, G., and Plemenos, D. (2010). Incorporating Viewpoint Entropy into the S-PDB viewer for Selecting Optimal 3D object Views. *International Conference on Computer Graphics and Artificial Intelligence (3ia), Athens, Greece*.

Feixas, M., Sbert, M., and González, F. (2009). A Unified Information-Theoretic Framework for Viewpoint Selection and Mesh Saliency. *ACM Transactions on Applied Perception*, 6(1).

Hartwig, S., Schelling, M., v. Onzenoodt, C., Vázquez, P.-P., Hermosilla, P., and Ropinski, T. (2022). Learning Human Viewpoint Preferences from Sparsely Annotated Models. *Computer Graphics Forum*, 41(6):453–466.

Heinrich, J., Vuong, J., Hammang, C. J., Wu, A., Rittenbruch, M., Hogan, J., Brereton, M., and O'Donoghue,

S. I. (2016). Evaluating Viewpoint Entropy for Ribbon Representation of Protein Structure. *Computer Graphics Forum*, 35(3):181–190.

Kamada, T. and Kawai, S. (1988). A simple method for computing general position in displaying three-dimensional objects. *Computer Vision, Graphics, and Image Processing*, 41(1):43–56.

Kouřil, D., Strnad, O., Mindek, P., Halladjian, S., Isenberg, T., Gröller, M. E., and Viola, I. (2021). Molecumentary: Scalable Narrated Documentaries Using Molecular Visualization. *IEEE Transactions on Visualization and Computer Graphics*, pages 1–1.

Kozlíková, B., Krone, M., Falk, M., Lindow, N., Baaden, M., Baum, D., Viola, I., Parulek, J., and Hege, H.-C. (2017). Visualization of Biomolecular Structures: State of the Art Revisited. *Computer Graphics Forum*, 36(8):178–204.

Larroque, V., Maria, M., Mérillou, S., and Montes, M. (2023). Automatic Molecular Tour Creation: A Study. In Singh, G. and Chu, M. R., editors, *Eurographics 2023 - Posters*. The Eurographics Association.

Lasseter, J. (1987). Principles of traditional animation applied to 3D computer animation. In *Proceedings of the 14th Annual Conference on Computer Graphics and Interactive Techniques*, SIGGRAPH '87, pages 35–44, New York, NY, USA. Association for Computing Machinery.

Marsaglia, N., Kawakami, Y., Schwartz, S. D., Fields, S., and Childs, H. (2021). An Entropy-Based Approach for Identifying User-Preferred Camera Positions. In *2021 IEEE 11th Symposium on Large Data Analysis and Visualization (LDAV)*, pages 73–83.

Olson, A. J. (2018). Perspectives on Structural Molecular Biology Visualization: From Past to Present. *Journal of Molecular Biology*, 430(21):3997–4012.

Plemenos, D. and Benayada, M. (1996). Intelligent Display in Scene Modeling. New Techniques to Automatically Compute Good Views. In *In Proceedings of the International Conference GraphiCon'96*, St Petersbourg, Russia.

Polonsky, O., Patané, G., Biasotti, S., Gotsman, C., and Spagnuolo, M. (2005). What's in an image? *The Visual Computer*, 21(8):840–847.

Preim, B. and Meuschke, M. (2022). A survey of medical animations. *Computers & Graphics*, 107:304–328.

Saleem, W., Song, W., Belyaev, A., and Seidel, H.-P. (2007). On computing best fly. In *Proceedings of the 23rd Spring Conference on Computer Graphics*, SCCG '07, pages 115–121, New York, NY, USA. Association for Computing Machinery.

Sbert, M., Plemenos, D., Feixas, M., and González, F. (2005). Viewpoint quality: Measures and applications. In *Proceedings of the First Eurographics Conference on Computational Aesthetics in Graphics, Visualization and Imaging*, Computational Aesthetics'05, pages 185–192, Goslar, DEU. Eurographics Association.

Schelling, M., Hermosilla, P., Vázquez, P.-P., and Ropinski, T. (2021). Enabling Viewpoint Learning through Dynamic Label Generation. *Computer Graphics Forum*, 40(2):413–423.

Secord, A., Lu, J., Finkelstein, A., Singh, M., and Nealen, A. (2011). Perceptual Models of Viewpoint Preference. *ACM Transactions on Graphics*, 30(5):1–12.

Shannon, C. E. (1948). A mathematical theory of communication. *The Bell System Technical Journal*, 27(3):379–423.

Sokolov, D. and Plemenos, D. (2008). Virtual world explorations by using topological and semantic knowledge. *The Visual Computer*, 24(3):173–185.

Sokolov, D., Plemenos, D., and Tamine, K. (2006). Methods and data structures for virtual world exploration. *The Visual Computer*, 22(7):506–516.

Stoev, S. and Straßer, W. (2002). A case study on automatic camera placement and motion for visualizing historical data. In *IEEE Visualization, 2002. VIS 2002.*, pages 545–548.

Trellet, M., Ferey, N., Baaden, M., and Bourdot, P. (2015). Content and task based navigation for structural biology in 3D environments. In *2015 IEEE 1st International Workshop on Virtual and Augmented Reality for Molecular Science (VARMS@IEEEVR)*, pages 31–36.

Vázquez, P.-P. (2009). Automatic view selection through depth-based view stability analysis. *The Visual Computer*, 25(5):441–449.

Vázquez, P.-P., Feixas, M., Sbert, M., and Heidrich, W. (2001). Viewpoint Selection Using Viewpoint Entropy: Automatic View Selection. In *Proceedings of the Vision Modeling and Visualization Conference 2001*, volume 22 of *VMV '01*, pages 273–280. Aka GmbH.

Vázquez, P.-P., Feixas, M., Sbert, M., and Llobet, A. (2002). Viewpoint entropy: A new tool for obtaining good views of molecules. In *Proceedings of the Symposium on Data Visualisation 2002*, VISSYM '02, pages 183–188, Goslar, DEU. Eurographics Association.

Vieira, T., Bordignon, A., Peixoto, A., Tavares, G., Lopes, H., Velho, L., and Lewiner, T. (2009). Learning good views through intelligent galleries. *Computer Graphics Forum*, 28(2):717–726.

Xie, K., Yang, H., Huang, S., Lischinski, D., Christie, M., Xu, K., Gong, M., Cohen-Or, D., and Huang, H. (2018). Creating and chaining camera moves for quadrotor videography. *ACM Transactions on Graphics*, 37(4):88:1–88:13.

APPENDIX

Table A1 gives the symbols used to define the metrics presented in sections A to E.

Table A1: Common symbols for presented metrics.

Notation	Description
$VQ_n(v)$	Viewpoint quality (of viewpoint) v
v	a viewpoint
V	the set of viewpoints
c	a turning angle of the silhouette
C_v	the set of turning angles of the silhouette seen from v
N_c	the size of C_v
e	an element (atom or bond)
E	a set of elements
$a_e(v)$	projected surface of e on v
$a_t(v)$	projected surface of the visualized molecule on v
$A_e(v)$	real surface of element e
$A_t(v)$	real surface of the visualized molecule
$p(e\,\|\,v) = \frac{a_e(v)}{a_t(v)}$	probability of a element e to appear on v
$p(e) = \sum_{v \in V} p(v)p(e\,\|\,v)$	probability of element e
$p(v) = \frac{a_t(v)}{\sum_{v \in V} a_t(v)}$	probability of viewpoint v
D_v	the set of depth seen from viewpoint v

A Silhouette Metrics

Some metrics of this category use symbols defined in table A1.

Silhouette Length. (Polonsky et al., 2005)

$$VQ_1(v) = \text{slength}(v)$$

With $slength(v)$ the number of pixels of the silhouette of the molecule seen from v.

Silhouette Entropy. (Polonsky et al., 2005)

$$VQ_2(v) = -\sum_{\alpha \in A_c} h(\alpha) \log h(\alpha)$$

With A_c the classes from the turning angle histogram h. At its maximum, this metric captures a highly curved silhouette.

Silhouette Curvature. (Vieira et al., 2009)

$$VQ_3(v) = \frac{\sum_{c \in C_v} \frac{|c|}{\frac{\pi}{2}}}{N_c}$$

This metric is maximized when the silhouette is highly curved and minimized with a flat silhouette.

Silhouette Curvature Extrema. (Secord et al., 2011)

$$VQ_4(v) = \frac{\sum_{c \in C_v} \left(\frac{|c|}{\frac{\pi}{2}}\right)^2}{N_c}$$

This metric amplifies curved silhouettes even more than *Silhouette curvature* because of the squared factor.

B Surface Metrics

Most surface metrics use the common symbols in table A1.

# of Visible Elements. (Plemenos and Benayada, 1996)

$$VQ_5(v) = \sum_{e \in E} vis_e(v)$$

With $vis_e(v) = 1$ if e is visible from v else 0. Corresponds to the total number of atoms or bonds visible from v.

Projected Surface. (Plemenos and Benayada, 1996)

$$VQ_6(v) = a_t(v)$$

The projected surface of the visualized molecule on viewpoint v.

Plemenos and Benayada. (Plemenos and Benayada, 1996)

$$VQ_7(v) = \frac{VQ_5(v)}{N_e} + \frac{VQ_6(v)}{R}$$

With N_e the total number of elements and R the total number of pixels of the input image. This metric is the combination of ratios of visible elements and total projected surface.

Visibility Ratio. (Plemenos and Benayada, 1996)

$$VQ_8(v) = \frac{\sum_{e \in E} vis_e(v) A_e}{A_t}$$

The ratio of the real area of visible elements and the total real surface of the molecule.

Viewpoint Entropy. (Vázquez et al., 2002)

$$VQ_9(v) = -\sum_{e \in E} p(e|v) \log p(e|v)$$

The entropy of probabilities that an element is visible on viewpoint v. Most entropy-based metrics are sensitive to the number of elements that are visible from the evaluated viewpoint. This is because when there are a lot of smaller elements on an image their probabilities to appear on v decreases.

Kullback-Leibler Distance. (Sbert et al., 2005)

$$VQ_{10}(v) = \sum_{e \in E} p(e|v) \log \frac{p(e|v)}{\frac{A_e}{A_t}}$$

The Kullback-Leibler divergence between the visible surface and the real surface of elements visible from v.

Viewpoint Mutual Information. (Feixas et al., 2009)

$$VQ_{11}(v) = \sum_{e \in E} p(e|v) \log \frac{p(e|v)}{p(e)}$$

This metric seeks to expose viewpoints where elements are exclusive to it on its high scores. On low scores, it gives viewpoints with elements representative of the observed molecule.

Information I_2. (Bonaventura et al., 2011)

$$VQ_{12}(v) = -\sum_{e \in E} p(e) \log p(e) - VQ_9(v)$$

This metric compares the entropy of all elements of the molecule and the entropy of the current viewpoint. Because the information of all elements is constant for a given molecule, this metric depends on *Viewpoint entropy*. Both metrics have the same general behavior but *Information* I_2 is more stable when visualizing more elements.

Information I_3. (Bonaventura et al., 2011)

$$VQ_{13}(v) = \sum_{e \in E} p(e|v) I_2(V;e)$$

$$I_2(V;e) = -\sum_{v \in V} p(v) \log p(v) + \sum_{v \in V} p(v|e) \log p(v|e)$$

With $p(v|e) = \frac{p(v)p(e|v)}{p(e)}$. When maximized, this metric shows the maximum number of most informative elements which are elements that can be seen from many viewpoints.

C Depth Metrics

Some depth metrics use symbols defined in table A1.

Maximum Depth. (Secord et al., 2011)

$$VQ_{14}(v) = \max_{d \in D_v} d$$

The maximum depth value from a viewpoint v.

Stoev and Straßer. (Stoev and Straßer, 2002)

$$VQ_{15}(v) = \alpha\, p(v) + \beta\, d(v) + \gamma(1 - |d(v) - p(v)|)$$

With $p(v)$ the normalized projected surface and $d(v)$ the maximum normalized depth from v. The authors recommend $\alpha = \beta = \gamma = \frac{1}{3}$ for general purposes.

Depth Distribution. (Secord et al., 2011)

$$VQ_{16}(v) = 1 - \sum_{d \in D_c} h(d)^2$$

With D_c the classes from the depth histogram h. This metric has a viewpoint with a big range of depth visible on its high score and a viewpoint with balanced depth values on low scores.

Depth Entropy. (Marsaglia et al., 2021)

$$VQ_{17}(v) = -\sum_{d \in D_v} p(d) \log p(d)$$

With $p(d)$ the probability of depth d. It has the same behavior as *Depth distribution*.

D Stability Metrics

Instability. (Feixas et al., 2009)

$$VQ_{18}(v) = \frac{1}{N_v} \sum_{j=1}^{N_v} \mathrm{JS}(w_i, w_j; p(E|v), p(E|v_j))$$

$$w_i = \frac{p(v)}{p(v) + p(v_j)} \qquad w_j = \frac{p(v_j)}{p(v) + p(v_j)}$$

With JS the Jensen-Shannon divergence, N_v is the number of neighboring viewpoints of v and $p(E|v)$ the probabilities of all elements E on v. This metric measures the distance of the distribution of elements between v_i and v_j. *Instability* shows a viewpoint with the most similar neighbors when minimized.

Depth-Based Visual Stability. (Vázquez, 2009)

$$VQ_{19}(v) = \frac{1}{\#V} \sum_{v_j \in V \setminus \{v\}} \mathrm{NCD}(v, v_j)$$

$$\mathrm{NCD}(v_i, v_j) = \frac{L(v_i v_j) - \min\{L(v_i), L(v_j)\}}{\max\{L(v_i), L(v_j)\}}$$

With NCD the normalized compression distance, $\#V$ the number of viewpoints, $L(v)$ the size of the compressed image of viewpoint v, $v_i v_j$ the concatenated image of viewpoint v_i and v_j. We observed that using threshold values as (Vázquez, 2009) recommends to compute the number of similar viewpoints leads to many viewpoints with the same score for molecules. This is why we instead opted to use the mean of the NCDs to avoid this issue. Viewpoints with a lot of similar viewpoints have higher scores.

E High-Level Metrics

Largest Cone of View.

$$VQ_{20}(v) = \max_{c \in C} (r_c - ||pos_c - pos_v||)$$

With r_c and pos_c respectively, the radius and center of circumcircle c from the circumcircle set C and pos_v the position of viewpoint v. This formulation, inspired by (Trellet et al., 2015), gives higher scores to viewpoints close to large cones of view.

F Molecular Dataset

The table A2 gives the PDB IDs (Berman et al., 2000) of molecules used in this study.

Table A2: Molecules PDB IDs (Berman et al., 2000) used in this study.

Tunnel dataset (33 elements)
1A0S, 1A2V, 1A6R, 1AON, 1AW5, 1BHC, 1CGM, 1EI7, 1GRL, 2GTL, 2X2C, 4V4K, 5CQF, 6QZ9, 6U42, 6U5F, 6X62, 6X63, 6X6K, 6ZW7, 7AX3, 7AZD, 7LER, 7MUS, 7PKR, 7Q4U, 7QXF, 7R5J, 7SN9, 7SP4, 7SQC, 7T7C, 7TBI

Alignment dataset (30 elements)
1A3J, 1AGA, 2ONX, 3DG1, 3FPO, 3FVA, 3NVG, 3OVL, 4NIO, 4QXX, 4R0P, 4RIL, 4W5M, 4W71, 4XFO, 5E5Z, 5I55, 5K2E, 5TXD, 6BZM, 6C3F, 6C3S, 6C4O, 6DIY, 6FGR, 6FHD, 6NB9, 6RHB, 7LTU, 8DDG